



Sakarya University Journal of Science

ISSN 1301-4048 | e-ISSN 2147-835X | Period Bimonthly | Founded: 1997 | Publisher Sakarya University |

<http://www.saujs.sakarya.edu.tr/>

Title: Autonomous flight performance improvement of the morphing aerial robot by aerodynamic shape redesign

Authors: Harun Çelik, Tuğrul Oktay, Metin Uzun

Received: 2017-12-05 17:51:14

Revised: 2018-09-13 11:09:12

Accepted: 2018-10-06 02:10:31

Article Type: Research Article

Volume: 23

Issue: 1

Month: February

Year: 2019

Pages: 51-65

How to cite

Harun Çelik, Tuğrul Oktay, Metin Uzun; (2019), Autonomous flight performance improvement of the morphing aerial robot by aerodynamic shape redesign. Sakarya University Journal of Science, 23(1), 51-65, DOI: 10.16984/saufenbilder.362588

Access link

<http://www.saujs.sakarya.edu.tr/issue/38708/362588>

New submission to SAUJS

<http://dergipark.gov.tr/journal/1115/submission/start>

Autonomous flight performance improvement of a morphing aerial robot by aerodynamic shape redesign

Harun Çelik^{*1}, Tuğrul Oktay², Metin Uzun³

Abstract

In this article, autonomous flight performance of an unmanned aerial robot is advanced by benefiting aerodynamic nose and tail cone shapes redesign both experimentally and computationally. For this intention, aerodynamic performance criteria (i.e. maximum fineness) of a scaled model of autonomous aerial robot called as Zanka-II manufactured at Erciyes University Faculty of Aeronautics and Astronautics Model Aircraft Laboratory is first observed in subsonic Wind Tunnel. Results obtained in such wind tunnel are subsequently validated using computational fluid dynamic (CFD) software (i.e. Ansys). Therefore, nose and tail cone of fuselage are improved in order to improve maximum fineness of the autonomous aerial robot. Finally, a novel scaled model using optimum data is redesigned and placed in Wind Tunnel to validate Ansys results with experimental results. By using geometrical data of ultimate aerodynamically optimized aerial robot, better autonomous flight performance is achieved in both simulation environment (i.e. Matlab and Simulink) and real time flights.

Keywords: aerodynamic shape, aerial robots, autonomous performance, nose cone, tail cone

Nomenclature

α Angle of attack
 C_D Drag Coefficient
 C_L Lift Coefficient

CFD Computational Fluid Dynamic
 E_{max} Maximum fineness value
 J Cost function
 K_D Derivative gain
 K_I Internal gain

* Corresponding Author

¹ Department of Aircraft Electrics and Electronics, Erciyes University, 38038, Melikgazi, Kayseri/Turkey. E-mail: drharuncelik@gmail.com

² Department of Aeronautical Engineering, Erciyes University, Tukey.

³ Department of Airframe, Erciyes University, Tukey.

K_p	<i>Proportional gain</i>
PID	<i>Proportional–Integral–Derivative</i>
T_{rt}	<i>Rising time</i>
T_{st}	<i>Settling time</i>
$xwmp, xhmp$	<i>aerial morphing parameters</i>
WT	<i>Wind tunnel</i>
θ	<i>Pitching angle of Aerial Robot</i>
$\%OS$	<i>Percent overshoot</i>

1. INTRODUCTION

For around last five quarters, aerial robots have been largely performed for military tasks as well as in commercial operations because of the reality of that they have several eligibilities with respect to the traditional manned vehicles. Some of these eligibilities are cost-effective manufacturing and operation, not risking pilots on hazardous conditions, and elastic configuration for customer request.

Various aerial robots have been used in aerial agriculture; for instance, crop monitoring and spraying, coast guarding such as sea lane and coastline, photography, conservation such as land monitoring and pollution during civilian missions.

On the other hand, aerial robots have also been utilized for military operations. For example, they have been operated for navy such as decoying missiles via the emission of artificial signatures and shadowing enemy fleets; army such as surveillance and reconnaissance of enemy activity; and air force tasks such as radar system destruction and jamming, and airfield base security. Considerable diversity in the aerial

robots is proposed in detail by [1]. Additionally, various scientific researches on design, manufacturing and autonomous control of aerial robot have been currently investigated [2-7].

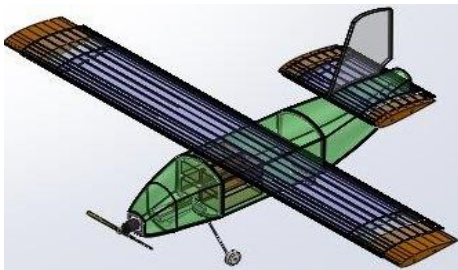
In order to obtain maximum performance for an air vehicle, several researches are conducted on aerodynamic shape improvement [8-11]. In Several tail cone shapes such as elliptical tail cone, conical tail cone and spherical tail cone are tested in order to reduce drag [9]. Also, optimal wing shapes are investigated to obtain minimum drag for an experimental unmanned aerial vehicle by using an aerodynamic shape improvement algorithm [10]. These studies show that 30% of wing drag reduction can be achieved by aerodynamic shape improvements. In another research, improvement of free-to-rotate tail fins are performed [11]. Both steady and unsteady asymmetric flows among its designs in canard fins are calculated by solving the Reynolds-Averaged Navier-Stokes solutions with Fluent [12-14]. The optimum tail fin reduced roll rate of the tail fins around 6%, and increased the normal force about 4%.

In aerodynamic shape improvement studies, this is the first journal article considering aerodynamic nose and tail cone shape improvement for performance improvement of autonomous aerial robot by simultaneous design of a load-carrying aerial robot and autopilot system. Moreover, a stochastic optimization method is first time benefited for this purpose, hence the optimum value of cost function is

found accurately and fast. In addition, although smaller values of overshoot, settling time and rise time are satisfied during tracked trajectory, aerodynamic nose and tail cone shape improvement advanced autonomous flight performance considerably [15].

2. MORPHING MECHANISM OF THE AERIAL ROBOT

Aerial robot wings yield the aerial robot to satisfy the flight conditions, but wings solely are not sufficient to satisfy the best flight performance in each condition. In order to achieve the optimal performance, mechanisms such as morphing flaps and wing tips that can change wing surface and aerial robot geometry during flight have studied by researchers and designers. After seeing accomplishment of these studies, placement of mechanical moving elements on the wing tips and remote control of wing tips are developed [16, 17]. In this study, both nose and tail cone of aerial robot are redesigned. Drawing of manufactured morphing aerial robot Zanka-II, and its side and upper view photos are illustrated in Figure 1.



(a)



(b)



(c)

Figure 1. Drawing of morphing aerial robot (morphing aspects are brown) (a), side (b) and upper view (c) photos of Zanka-II

Each one of the wing system comprises gear teeth, micro motor, bidirectional mini brushing electronic speed controller (ESC), and M3 worm gear. As seen in Figure 2 (a), micro motor is a DC motor and operating between ranges 6-9 V, creates a torque of 1.8 kg. The gear motor is placed on the shaft of the related motor (see Figure 2 (b)). This gear operates with a second gear placed on the bearing compatibly (see Figure 2 (d)). In released state of the gear mounted on bearing, the gear has M3 tooth. For turning the engine right or left by the remote control, a bistable switch is used to send signal to ESC (see Figure 2 (c)). ESC is a bidirectional and brushed circuit, and works in two sides in terms of the incoming signal directly through the

remote control switch (see Figure 2 (e)). The direction of gear rotation determines moving of motor, and hence a mechanical system that has such a gear can lead screw in-or-outward smoothly (see Figure 2(f)). This movement results to moving of wing tip parts, and therefore provides alteration of the wing area.



(a)



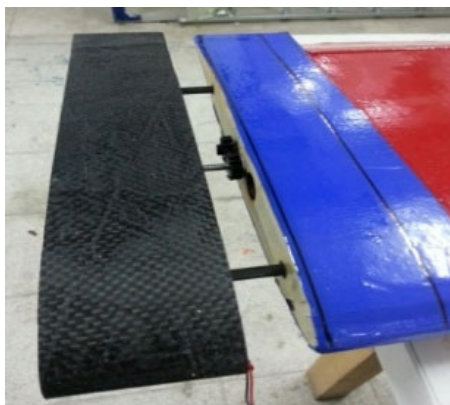
(b)



(c)



(d)



(e)



(f)

Figure 2. Morphing mechanism. DC (a) and gear motor (b) placed on shaft. Servo motor placement in the wing (c). Electronic speed controller (d). Assembly of the expanding parts of the wing (e). 3D view of the moving part of the wing (f)

3. AERODYNAMIC SHAPE IMPROVEMENT

Aerodynamic shape improvement of an air vehicle can be achieved by maximum fineness ratio that is a combination of the lift and drag forces of the air vehicle. An increase in the lift force of the air vehicle increases the controllability, hence the distance of take-off and landing decrease, and similarly the decrease in the drag force reduce fuel consumption. Maximum fineness ratio can be defined as the ratio of the lift force to the drag force in general expression. However, solely increasing the lift force or decreasing the drag force for performance improvement may not be sufficient, since the drag force is proportional to the square of the lift force as given in (1). Therefore, examining (2) can be more accurate and reliable for aerodynamic improvement.

$$C_D = C_{D_0} + KC_L^2 \quad (1)$$

$$E_{\max} = \frac{1}{2\sqrt{KC_{D_0}}} \quad (2)$$

where C_D and C_L are drag and lift coefficient. C_{D_0} depicts the drag force coefficient when the lift force is 0. $K = 1/(\pi A_R e)$ where A_R is wing aspect ratio, and e is oswald constant.

3.1. Numerical Method

Flight performance of an autonomous aerial robot improved by optimum aerodynamic nose and tail cone shape may be computationally investigated by using CFD code with commercial Ansys [20-22] software depended on finite volume technique [23]. The aerial robot has 1.06 m length and 1.60 m wingspan. For all simulations, velocity, density of air, and kinematic viscosity are defined as 16.6 m/s (about 100km/h), 1.036 kg/m³ and 1.5111x10⁻⁵ m²/s, respectively. Also, Angle of attack is selected as -4, 0, 4, 8, 12 and 16 degrees.

The turbulent viscosity was worked out through Standard k-ε Turbulence Model [24-26]. All solution variables were solved via first order upwind discretization scheme [27]. For these simulations, the convergence criterion is selected to be 10⁻⁶.

3.2. Boundary Condition

Computational domain extended to 15 wingspans (C) for upstream of the leading point and downstream of the trailing point of the aerial robot. Also 20 C was implemented from pressure outlet surface. Velocity inlet boundary condition was applied upstream and downstream with speed of 16.6 m/s. No-slip boundary condition is used at solid surfaces. Figure 3 illustrates all these properties for simulations. Velocity components are defined for each angle of attack situation. The x component of velocity is calculated by $x=16.6\cos\alpha$, and y component of velocity is defined with $y=16.6\sin\alpha$ formula, where α is the angle of attack in degree.

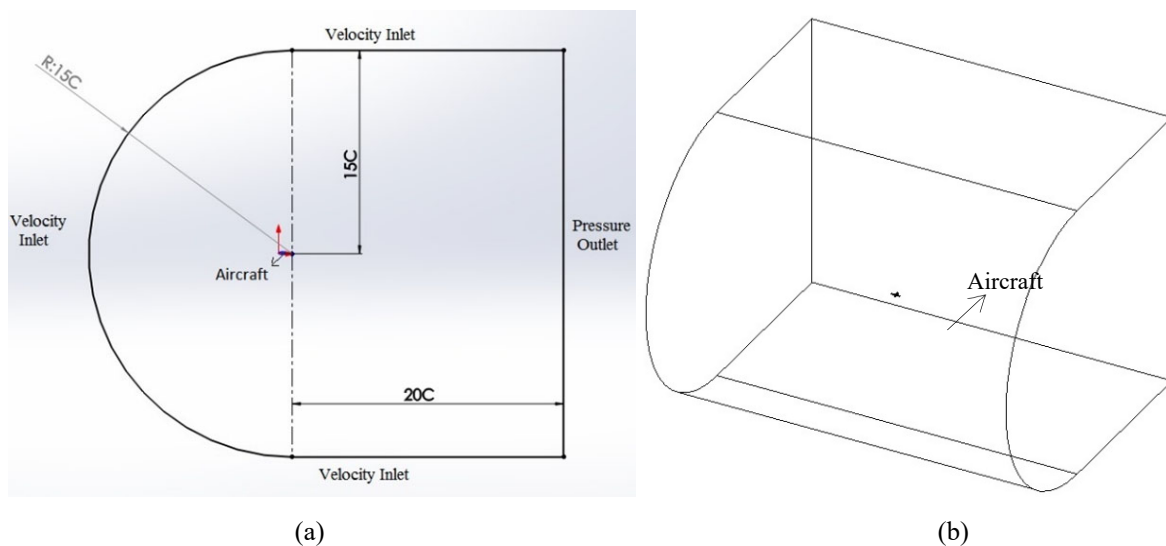


Figure 3. The dimensions (a) and boundary conditions (b) of the computational domain (nose and tail cone)

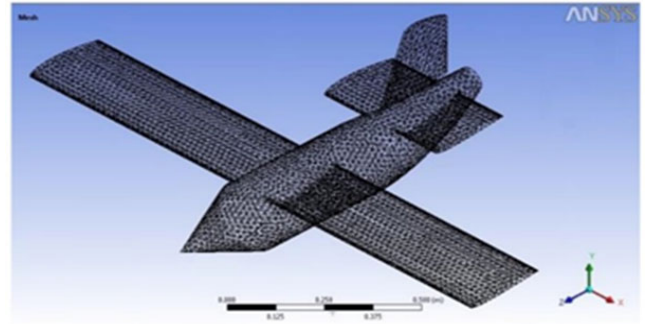
3.3. Grid Independency Study

The grid for simulations is generated by Ansys Mesh program, and nose options with mesh are shown in Figure 4. Patch conforming/sweeping method which is suitable for clean computer aided design geometries is used for meshing. For eliminating of mesh effects, optimum mesh element number should be determined. Increasing of the element number provides more accurate results, but using more element increases solving time. For this reason, grid independency study has been done with 0.1k, 0.4k, 1k, 2.4k, 6k and 10k elements where $k=10^6$. In Figure 5, lift coefficient (C_L) variation with different element numbers are given at 0 degree angle of attack. For elements number larger than 2.4k, lift coefficient values do not change considerably. So it can be decided that 2.4k elements are enough for the accurate results. Approximately all of these analyses completed between 10000 and 20000 iterations. Used computer for these analyses has 3.60 GHz CPU and 8 GB RAM. Maximum analysis time for a simulation was 2 hours. Similar to nose cone, all of these processes are reperformed for the tail cone.

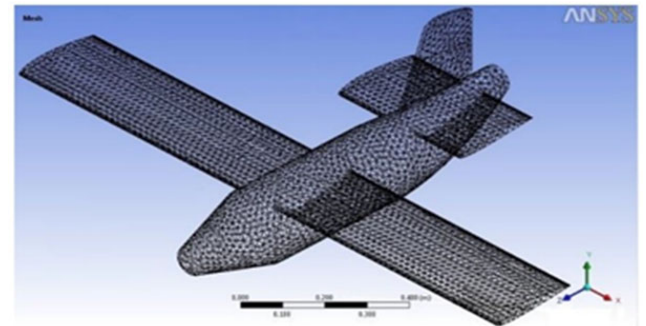
To summarize, in this section, various nose and tail cone equations have been examined to improve the autonomic performance of the aerial robot.

E_{max} values are calculated using various equations of nose and tail cone with both CFD and WT. Comparison results of CFD and WT are given in

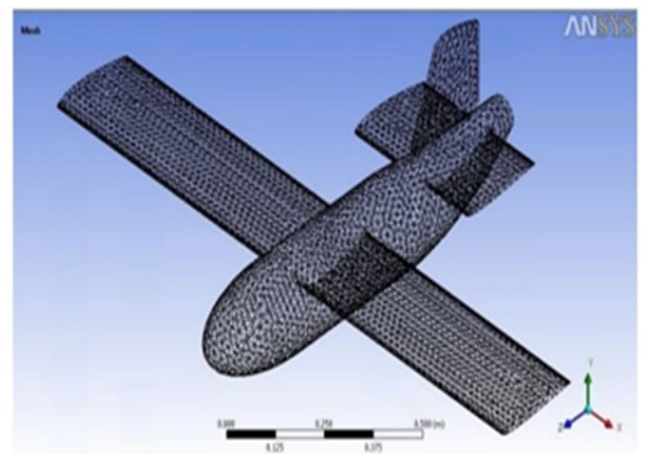
Table 1 and 2. Solid drawings of these various values performed in nose and tail cone equations are shown in Figure 4. The most appropriate equation for both nose and tail cone are obtained as conic equation with E_{max} value of 6.54 and 6.44, respectively.



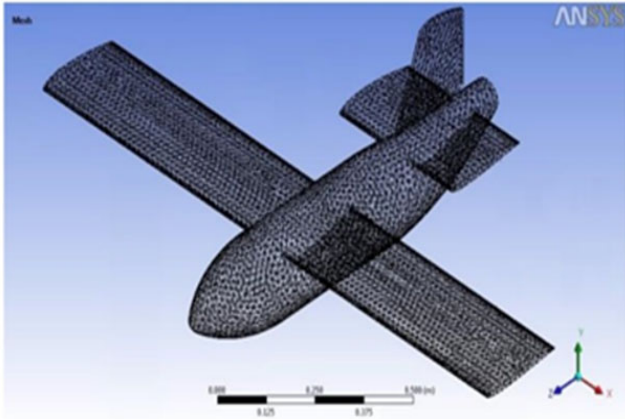
(a)



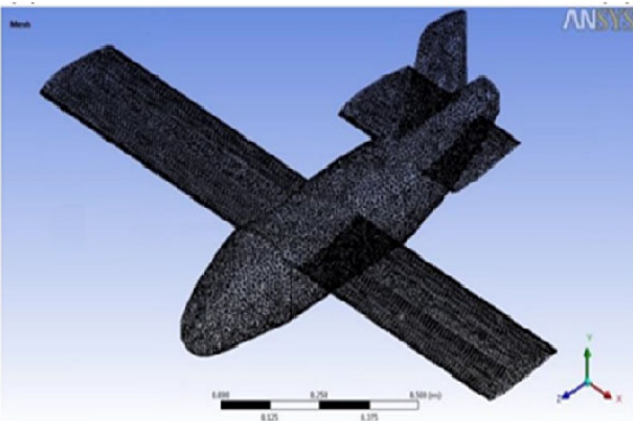
(b)



(c)



(d)



(e)

Figure 4. Mesh of nose options. Conical (a), Biconical (b), Elliptical (c), Spherically tangent ogive (d), Initial reference manufactured (e)

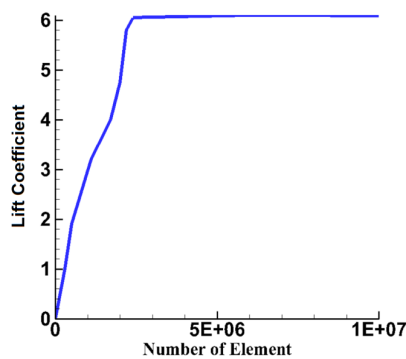
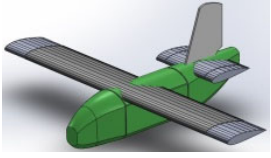
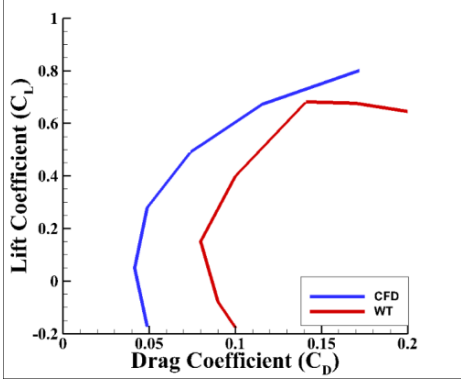
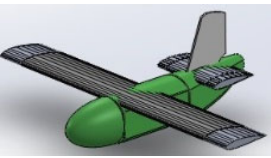
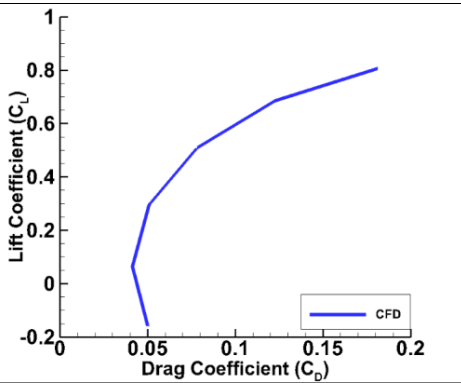
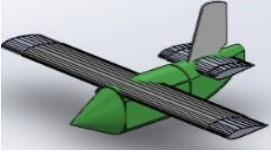
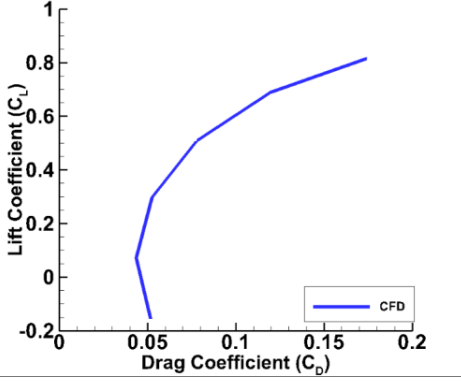
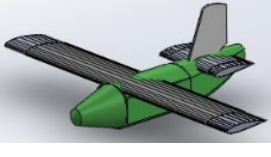
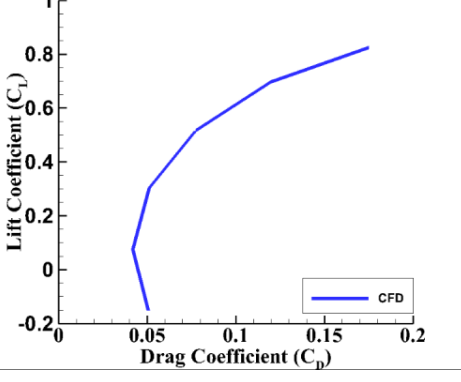


Figure 5. Grid independency result for lift coefficient (nose and tail cone)

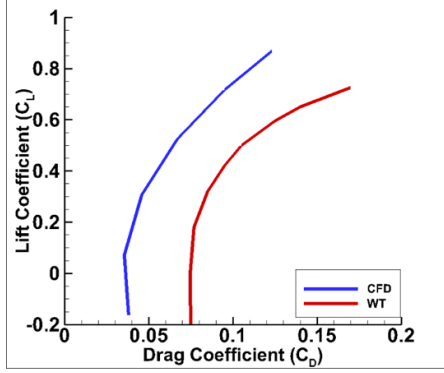
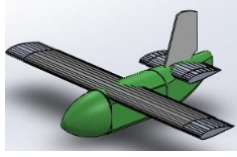
3.4. Aerodynamical Results

In this subsection, various nose and tail cone shapes such as elliptical, conical, biconical, inverse-parabolic, parabolic, spherically blunted tangent ogive, and haack series [18, 19] are investigated to maximize the value of maximum fineness (E_{max}). In Table 1 and 2, CFD drawings, CFD and Wind Tunnel (WT) results, and E_{max} values are presented for nose and tail cone shapes, respectively. From these tables, it can be seen that the maximum value of E_{max} is obtained for *spherically blunted tangent ogive* nose cone shape, and *conical* tail cone shape. The maximum values of E_{max} are around 1.4-3% larger than the one of initial reference aerial robot. This amount may seem smaller, but it has very important advantageous for performance characteristics such as maximum range, endurance and autonomous performance. It is important to state that initial cone and ultimate cone which has maximum E_{max} values (i.e. optimum geometry) are only experimented in wind tunnel. The maximum fineness value for the remainder of cones is expected computationally, so do not need to test with the aforementioned cone configurations. In Figure 6, wind tunnel experiments for initial and optimum geometry are presented.

Table 1. Improvement results for nose cone

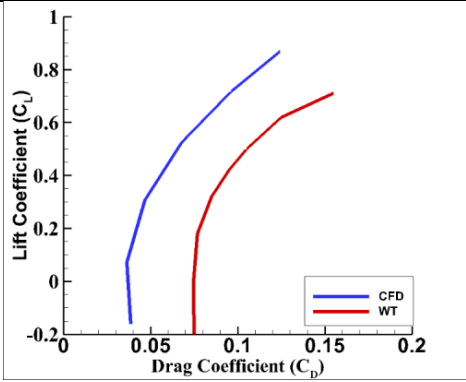
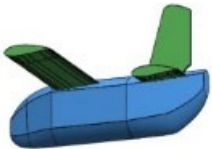
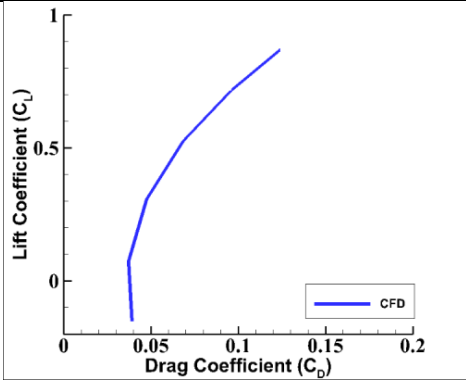
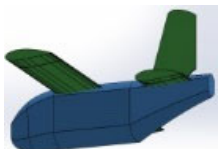
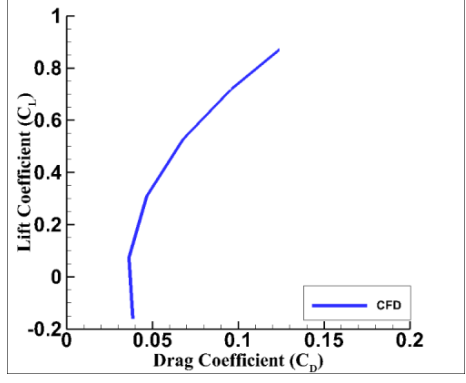
Nose cone	CFD	C_L - C_D	E_{max}
Produced Aircraft			6.35
Elliptical			6.33
Conical			6.22
Biconical			6.36

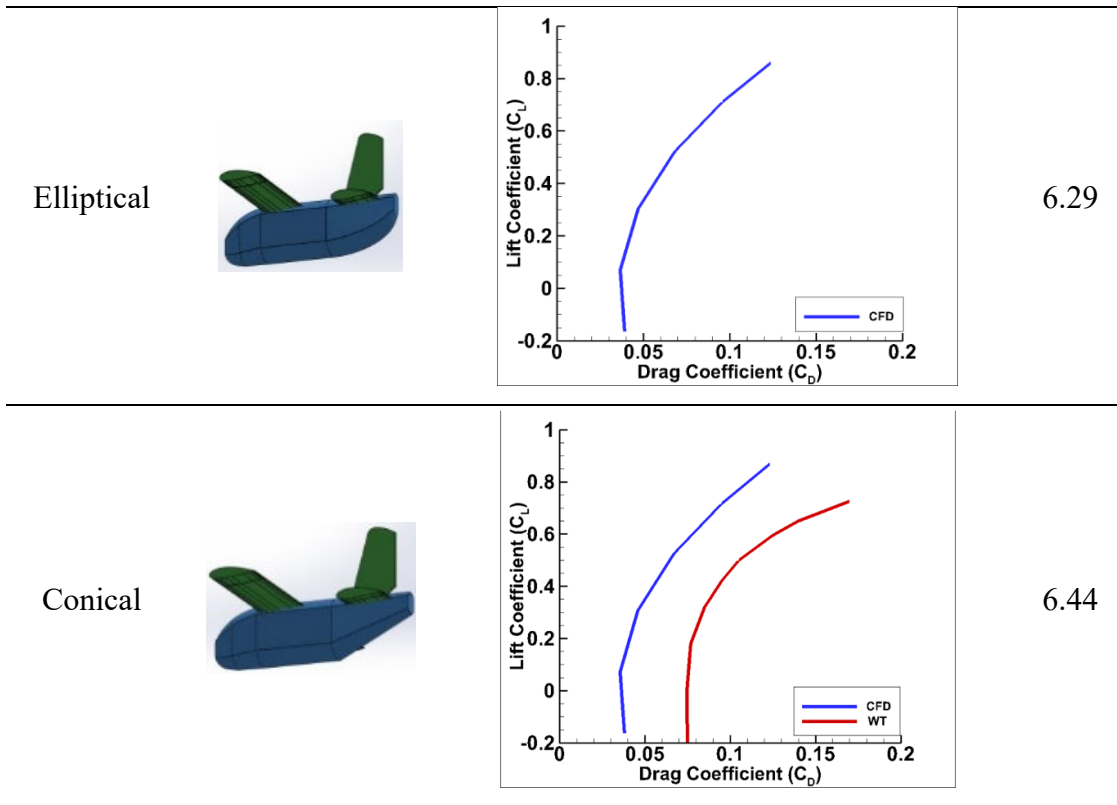
Spherically
Blunted
Tangent Ogive



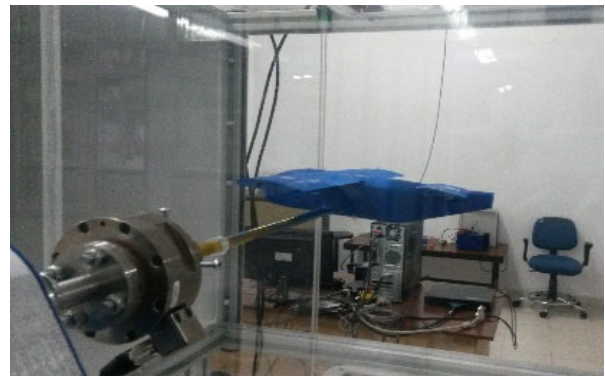
6.54

Table 2. Improvement results for tail cone

Tail cone	CFD	C_L - C_D	E_{max}
Produced Aircraft			6.35
Haack Series $C=0.3$			6.2
Inverse Parabolic			6.37



(a)



(b)

Figure 6. Wind Tunnel tests. Spherically blunted tangent ogive nose (a). Conical tail cone (b)

4. AUTOPILOT AND PERFORMANCE EVALUATION

4.1. Autopilot System

For both simulation environment (i.e. Matlab) and real-time flight study, classical PID based hierarchical autopilot system is chosen [28]. In the system structure, three layers of hierarchical PID

controller to satisfy tracking trajectory are performed as seen in

Figure 7. In this autopilot, control signals are provided by inner loop, desired pitch and yaw rates are achieved by middle loop, and the trajectory of aerial robot is tracked by outer loop. The T , h , r , ψ , θ , and ϕ indicate throttle, altitude, rudder, yaw, pitch and roll, respectively.

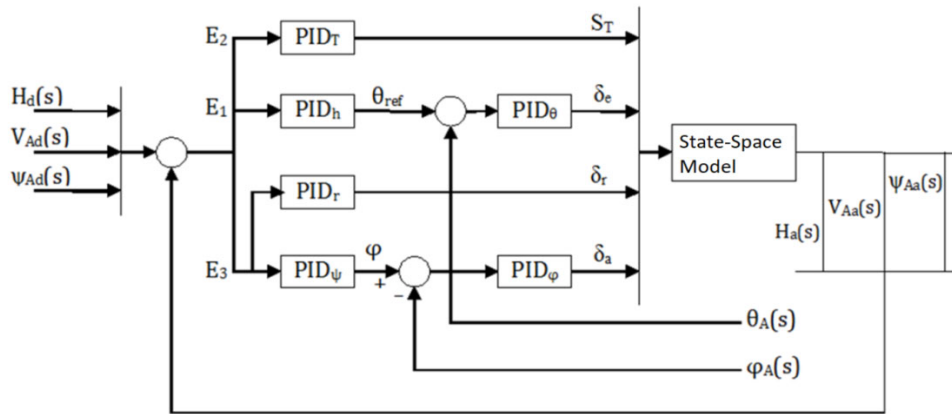


Figure 7. Hierarchical autopilot system

4.2. Autonomous Performance Evaluation

Generally, PID-based hierarchical controller system enables to control altitude, yaw angle, and velocity for tracking a definite trajectory. The proposed system includes 6 PID controllers with the 3 layers that are outer, middle, and inner loops. These PIDs have also upper and lower restrictions, and guarantee to track desired trajectory. For general situation, interested autopilot user needs to set totally 18 parameters of PID (i.e., 6 parameters for each P, I and D) to benefit from all internal PIDs. Moreover, in this study for simultaneous morphing aerial robot and autopilot design strategy, two more structural parameters (i.e. optimum extension ratios of horizontal tail and wing) are set. For high-performance trajectory tracking, a cost function consists of settling time (T_{st}), rise time (T_{rt}), and overshoot (OS) is defined as

$$J = \sum g(T_{st} - T_{st_u})^2 + g(T_{rt} - T_{rt_u})^2 + g(\%OS - \%OS_u)^2 \quad (3)$$

where subscript u denotes upper value; then optimization problem can be described as $\min\{J\}$

where J is the function of 20 terms (18 controller design parameters and 2 aerial morphing parameters) and can be given as

$$J = f \left(\begin{matrix} xwmp, xhmp, K_{P_1}, K_{I_1}, K_{D_1}, K_{P_2}, \\ K_{I_2}, K_{D_2}, \dots, K_{P_6}, K_{I_6}, K_{D_6} \end{matrix} \right) \quad (4)$$

where $xwmp$ and $xhmp$ are aerial morphing parameters, and K_P, K_I, K_D are autopilot

parameters for each PID. Terms of cost function is calculated by using simultaneous perturbation stochastic approximation (SPSA) [29, 30] as

$$\text{If } T_{st} \geq T_{st_u}, T_{st} \text{ is non-defined else} \quad (5)$$

$$T_{st} < T_{st_u}, T_{st} \text{ is its value}$$

$$\text{If } T_{rt} \geq T_{rt_u}, T_{rt} \text{ is non-defined else,} \quad (6)$$

$$T_{rt} < T_{rt_u}, T_{rt} \text{ is its value}$$

$$\text{If } \%OS \geq \%OS_u, \%OS \text{ is non-defined else} \quad (7)$$

$$\%OS < \%OS_u, \%OS \text{ is its value}$$

SPSA results of cost function J for the best nose (a) and tail (b) cone are given in Figure 8. After the simultaneous optimization process, 3% and 1.4% improvements in maximum values of E_{\max} result to 2.6% and 1.1% improvement in entire autonomous performance by using nose and tail cone redesign, respectively. These improvements of E_{\max} may seem small. However, the improvements are

obtained with a very small modification in aerial robot geometry, and it is very important in terms of controller performance since reducing flight energy consumption. After applying the design methodology, and when Von Karman turbulence [31] exists to model a flight condition closed to real, satisfactory tracking trajectory of the aerial robot for pitch angle is depicted in Figure 9.

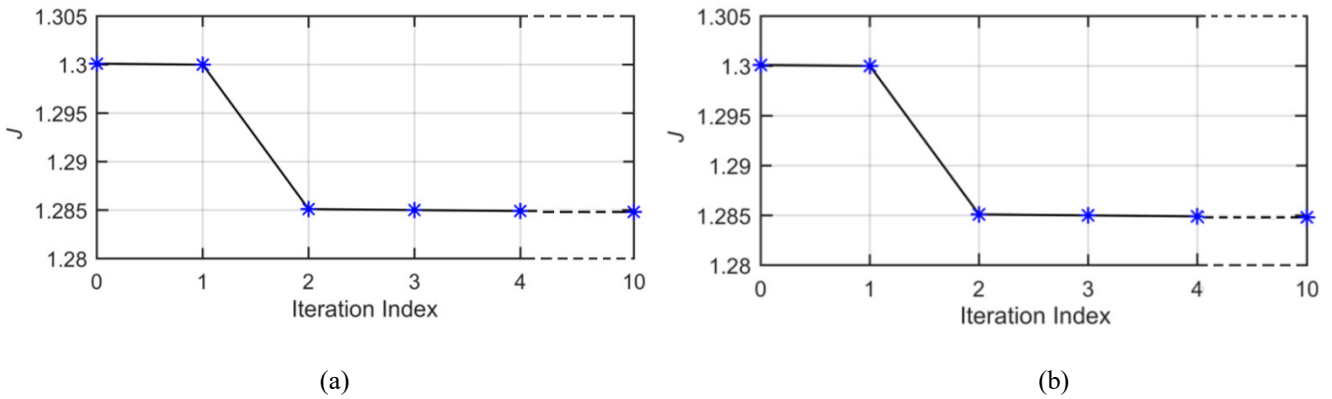


Figure 8. SPSA results of cost function J for the best nose (a) and tail (b) cone.

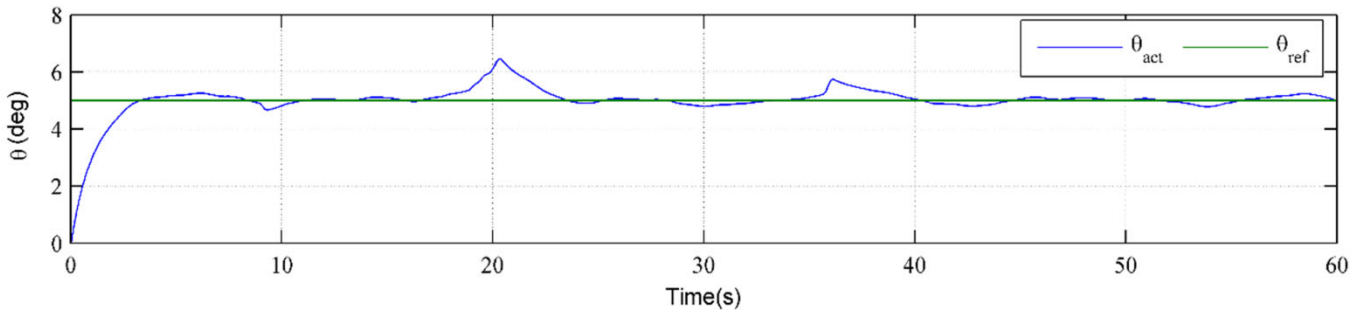


Figure 9. Trajectory tracking for resulting ultimate aerial robot

5. CONCLUSIONS

In order to improve flight performance of an autonomous aerial robot, aerodynamic nose shape optimization both experimentally and computationally were examined in this article. Aerodynamic performance criteria (i.e., maximum fineness) of a scaled model of the autonomous aerial robot manufactured at the Model Aircraft

Laboratory was first observed in subsonic Wind Tunnel. Obtained results were validated using a computational fluid dynamics software (i.e. Ansys). Nose and tail cone of fuselage were optimized in order to maximize maximum fineness of the autonomous aerial robot by using various shape equations in Ansys. After deciding the optimum shape, a new scaled model using the optimum data was then produced and placed in

Wind Tunnel in order to validate Ansys results with experimental results. By using geometrical data of ultimate aerodynamically optimized aerial robot, better autonomous flight performance was found both in simulation environment (i.e. Matlab) and real-time flight tests.

A small increase (around 3% and 1.4%, respectively) for the maximum value of fineness is obtained via aerodynamic nose and tail cone shape optimization for morphing autonomous aerial robot. Finally, a minor, but important, improvement (around 2.6% and 1.1%, respectively) in autonomous performance is achieved.

For the future, nose and tail cone can be investigated with a simultaneous design while it is studied separately in this article. Explicitly, each nose and tail cone shape is designed and then examined in computational fluid dynamic software and subsonic Wind Tunnel separately. In the future, various configurations of nose and tail cone can be examined at the same time. Thus, higher improvements can be achieved in autonomous performance.

ACKNOWLEDGMENTS

This work was supported by Research Fund of the Scientific and Technological Research Council of Turkey (TUBITAK) under Project Number: 214M282.

REFERENCES

- [1] R. Austin, *Unmanned aircraft systems*. Wiley, 2010.

- [2] Y. Ding, Y. C. Liu and F. B. Hsiao, "The application of extended Kalman filtering to autonomous formation flight of small UAV system," *Aircraft Engineering and Aerospace Technology*, vol. 1, no. 2, pp. 154-186, 2013.
- [3] A. Drak, M. Hejase, M. ElShorbagy, A. Wahyudie and H. Noura, "Autonomous Formation Flight Algorithm and Platform for Quadrotor UAVs," *International Journal of Robotics and Mechatronics*, vol. 1, no. 4, pp. 124-132, 2014.
- [4] L. De Filippis, G. Guglieri and F. B. Quagliotti, "A novel approach for trajectory tracking of UAVs," *Aircraft Engineering and Aerospace Technology: An International Journal*, vol. 86, no. 3, pp. 198 – 206, 2014.
- [5] T. Oktay, M. Uzun, H. Celik and M. Konar, "PID Based Hierarchical Autonomous System Performance Maximization of a Hybrid Unmanned Aerial Vehicle (HUAV)", *Anadolu University Journal of Science and Technology – A Applied Sciences and Engineering*, vol. 18, no. 3, pp. 554-562, 2017.
- [6] H. Celik, T. Oktay and I. Turkmen, "Model Predictive Control and Robustness Test of the Unmanned Aerial Vehicle (Zanka-I) in Various Turbulence", *Journal of Aeronautics and Space Technologies*, vol. 9, no. 1, pp. 31-42, 2016.

- [7] T. Oktay, and S. Coban, “Simultaneous Longitudinal and Lateral Flight Control Systems Design for Both Passive and Active Morphing UAVs,” *Elektronika ir Elektrotechnika*, vol. 23, no. 5, pp. 15-20, 2017.
- [8] Z. Xuetao, *UAV Design and Manufacture*, BS Thesis, 2010.
- [9] Z. Lyu, K. W. Kenway and J. R. Martins, “Aerodynamic Shape Optimization Investigations of the Common Research Model Wing Benchmark,” *AIAA Journal*, vol. 53, no. 4, pp. 968-985, 2015.
- [10] P. Gamboa, J. Vale, F. J. P. Lau and A. Suleman, “Optimization of a morphing wing based on coupled aerodynamic and structural constraints,” *AIAA journal*, vol. 47, no. 9, 2009.
- [11] E. Feyzioglu, “Roll characteristics and shape optimization of the free to-rotate tail-fins on a canard-controlled missile,” MS Thesis, Middle East Technical University, 2014.
- [12] R. P. Liem, J. R. Martins and G. K. Kenway, “Expected drag minimization for aerodynamic design optimization based on aircraft operational data,” *Aerospace Science and Technology*, vol. 63, pp. 344-362, 2017.
- [13] J. E. Hicken and D. W. Zingg, “Induced-Drag Minimization of Nonplanar Geometries Based on the Euler Equations,” *AIAA journal*, vol. 48, no. 11, 2010.
- [14] A. Khalid and P. Kumar, “Aerodynamic Optimization of Box Wing – A Case Study,” *International Journal of Aviation, Aeronautics, and Aerospace*, vol. 1, no. 4, 2014.
- [15] T. Oktay, M. Uzun, I. Yılmaz and M. Konar, “Aerodynamic nose shape optimization for performance maximization of morphing autonomous aerial robot,” *International Conference on Engineering and Natural Science*, Sarajevo, Bosnia and Herzegovina, 24-28 May 2016.
- [16] S. Barbarino, F. Gandhi and S. Webster, “Design of Extendable Chord Sections for Morphing Helicopter Rotor Blades,” *Journal of Intelligent Material Systems and Structures*, vol. 22, no. 9, pp. 891–905, 2011.
- [17] T. Yue and L. Wang, “Longitudinal Linear Parameter Varying Modeling and Simulation of Morphing Aircraft”, *AIAA Journal of Aircraft*, vol. 50, no. 6, pp. 1673-1681, 2013.
- [18] P. Neittaanmäki, T. Rossi, S. Korotov, E. Oñate, J. Périaux and D. Knörzer, “Overview on drag reduction technologies for civil transport aircraft,” European Congress on Computational Methods in Applied Sciences and Engineering (ECCOMAS), 24-28, July 2004.
- [19] M. K. Chan, “Supersonic Aircraft Optimization for Minimizing Drag and Sonic Boom,” PhD Thesis, 2003.

- [20] S. Fu and L. Wang, "Modelling the flow transition in supersonic boundary layer with a new $k-\omega-\gamma$ transition/turbulence model," *7th International Symposium on Engineering Turbulence Modelling and Measurements-ETMM7*, Limassol, Cyprus, 4–6 June, 2008.
- [21] F. Menter, "Two-equation eddy viscosity turbulence models for engineering applications," *AIAA Journal*, vol. 32, pp. 1598–1605, 1994.
- [22] R. E. Mayle and A. Schulz, "The path to predicting bypass transition," *ASME J. Turbomach*, vol. 119, pp. 405–411, 1997.
- [23] D. Choudhury, "Introduction to the renormalization group method and turbulence modeling," *Fluent Inc. Technical Memorandum*, TM-107, 1993.
- [24] D. D. Sanders, W. F. O'Brien, R. Sondergaard, M. D. Polanka and D. C. Rabe, "Predicting Separation and Transitional Flow in Turbine Blades at Low Reynolds Numbers-Part I: Development of Prediction Methodology," *J Turbomach*, vol. 133, pp. 1-10, 2010.
- [25] P. Catalano and R. Tognaccini, "Turbulence modeling for low Reynolds number flows," *AIAA Journal*, vol. 48, pp. 1673-1685, 2010.
- [26] F. R. Menter, R. B. Langtry, S.R. Likki, Y. B. Suzen, P. G. Huang and S. Völker, "A correlation based transition model using local variables: part I-model formulation," *Proceedings of ASME Turbo Expo 2004*, Vienna, Austria, pp. 57–67, 2004.
- [27] T. Misaka and S. Obayashi, "A correlation-based transition models to flows around wings," *AIAA Paper 2006–918*, 2006.
- [28] H. Chao, Y. Cao and Y. Q. Chen, *Autopilots for Small Fixed-Wing Unmanned Aerial Vehicles: A Survey. IEEE International Conference on Mechatronics and Automation*, Harbin, China, 2007.
- [29] J. C. Spall, "Multivariate stochastic approximation using a simultaneous perturbation gradient approximation," *IEEE transactions on automatic control*, vol. 37, no. 3, pp. 332-341, 1992.
- [30] T. Oktay, H. Çelik and M. Uzun, "A novel learning algorithm to estimate the optimum fuselage drag coefficient," *Sakarya University Journal of Science*, vol. 21, no. 1, pp. 63-68, 2017.
- [31] U.S. Military Handbook MIL-HDBK-1797, 19 December 1997.